

# Influence of the carrier on steam reforming of acetic acid over Ru-based catalysts

Aristides C. Basagiannis, Xenophon E. Verykios \*

*Department of Chemical Engineering, University of Patras, GR-26500 Patras, Greece*

Received 24 September 2007; received in revised form 29 December 2007; accepted 15 January 2008

Available online 20 January 2008

## Abstract

The reaction of steam reforming of acetic acid (HAc), a model compound of pyrolysis-oil, over ruthenium catalysts supported on  $\text{Al}_2\text{O}_3$  and  $\text{MgO}/\text{Al}_2\text{O}_3$  carriers has been investigated employing transient and steady-state techniques. Main objective is the establishment of the reaction network over a wide temperature range and the elucidation of the role of MgO on intrinsic catalytic activity. It has been found that the solid-state reaction of alumina with magnesium oxide is complete, forming magnesium aluminate spinel. This carrier interacts with acetic acid and promotes mainly the ketonization reaction and, secondarily, decomposition reactions. In the presence of Ru, catalytic activity is shifted towards lower temperatures and hydrogen production occurs at high rates. Ru catalysts promote the steam-reforming reaction and retard the rate of carbon deposition onto the catalytic surface. The magnesium aluminate spinel was found to be more resistant to coke deposition compared to alumina itself. Accordingly, the  $\text{Ru}/\text{MgO}/\text{Al}_2\text{O}_3$  catalyst exhibited the lowest rate of carbon deposition and was found to be significantly more active than the  $\text{Ru}/\text{Al}_2\text{O}_3$  catalyst, especially at lower temperatures. The enhanced activity of the  $\text{Ru}/\text{MgO}/\text{Al}_2\text{O}_3$  catalyst seems to be associated with the fact that the magnesium aluminate spinel offers enhanced O and/or  $-\text{OH}$  anion spillover from the carrier onto the metal particles and exhibits reduced surface acidity, as compared to the alumina carrier.

© 2008 Elsevier B.V. All rights reserved.

**Keywords:** Pyrolysis-oil; Acetic acid; Steam reforming; Hydrogen production; Magnesium aluminate spinel; Ruthenium catalysts

## 1. Introduction

There is currently significant interest for the production of hydrogen for energy applications, especially hydrogen originating from renewable sources. Although the development of fuel cells meeting the criteria of high efficiency, portability and affordability faces significant technical challenges, a major hurdle remains the sourcing of hydrogen and the development of efficient, safe and affordable production processes. At present, there are many well-established processes for hydrogen production from fossil fuels, such as naphtha, natural gas and coal [1]. However, real environmental benefits are linked with the ability to produce hydrogen from renewable sources, with no net production of greenhouse gasses. A viable renewable source, gaining attention in recent years, is bio-fuels. In this respect, many reports have dealt with the steam

reforming of bio-ethanol [2–6]. Renewable lignocellulosic biomass can also be used as an alternative feedstock for hydrogen production. A technology which has been explored in recent years is the catalytic steam reforming of pyrolysis-oil. This route involves pyrolysis of biomass to generate bio-oil, and reformation of it to produce a gaseous stream rich in hydrogen. New developments in flash pyrolysis technologies make it possible to convert biomass more efficiently into bio-oil [7,8], making it an attractive alternative intermediate for hydrogen production.

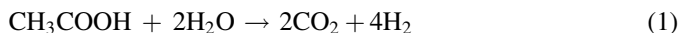
Pyrolysis-oil is a complex mixture of organic oxygenates, but its main components are more or less similar, independent of its source. Elementary analysis of bio-oil derived from different processes shows that its main components include: acids, alcohols, aldehydes, esters, ketones, sugars and phenols [9–11]. A number of studies dealing with the subject of reformation of bio-oil, using either bio-oil itself or model compounds, have been reported recently [12–20].

Acetic acid (HAc) is one of the major components of bio-oil (up to 12%) [9,10,21] and, for this reason it is often used as a

\* Corresponding author. Tel.: +30 2610 991527; fax: +30 2610 991527.

E-mail address: [verykios@chemeng.upatras.gr](mailto:verykios@chemeng.upatras.gr) (X.E. Verykios).

model compound. The steam reforming of acetic acid and the water gas shift reactions occur simultaneously, and the overall stoichiometry is represented by



Steam reforming of HAc is an endothermic reaction ( $\Delta H = 134.77$  kJ/mol at 298 K) which is entirely feasible from a thermodynamic point of view.

In a previous communication, it was reported that Ru-based catalysts, especially Ru supported on magnesia/alumina carrier, present high activity and high hydrogen selectivity as well as stable performance with time on stream [22]. Thus, aim of the present work was to investigate the reaction network of steam reforming of HAc over ruthenium catalysts over a wide temperature range, as well as to elucidate the role of MgO addition on  $\text{Al}_2\text{O}_3$  on catalytic performance.

## 2. Experimental

### 2.1. Catalyst preparation and characterization

The  $\text{Al}_2\text{O}_3$  carrier used in the preparation of catalysts is commercially available (Alfa Aesar). The  $\text{MgO}/\text{Al}_2\text{O}_3$  support, as well as the  $\text{Ru}/\text{Al}_2\text{O}_3$  and  $\text{Ru}/\text{MgO}/\text{Al}_2\text{O}_3$  catalysts were synthesized by the wet-impregnation method, using  $\text{Mg}(\text{NO}_3)_2$  and  $\text{Ru}(\text{NO})(\text{NO}_3)_3$  (Alfa Aesar) as Mg and Ru precursors, respectively. The MgO content in the  $\text{MgO}/\text{Al}_2\text{O}_3$  carrier was 15% by mass, while the nominal ruthenium loading in the Ru-based catalysts was 5%. Preparation of the materials has been presented in detail elsewhere [22].

Carriers and catalysts were characterized with respect to their specific surface area, exposed metallic surface area and crystallite size, employing techniques such as nitrogen physisorption (BET method), hydrogen chemisorption and X-ray diffraction (XRD) [22].

### 2.2. Apparatus

#### 2.2.1. Transient experiments

Transient experiments were carried out in an apparatus consisting of a flow switching system, a heated reactor and an analysis system. The flow apparatus has been described in detail elsewhere [23]. The reactor consists of two 6.0-mm OD sections of quartz tube, which serve as inlet and outlet to and from a quartz cell of 8.0-mm OD. The total length of the reactor is 32.0 cm. The catalyst sample, approximately 100 mg, was placed in the cell and kept in place by means of quartz wool. The temperature of the catalyst was measured at the inlet of the catalyst bed by means of a K-type thermocouple placed within a quartz capillary well. An electric furnace controlled by a programmable controller provided heating to the reactor. Analysis of the gases was done by on-line mass spectrometer (VG Quadrupoles, Sensorlab 200D) equipped with a fast response inlet capillary/leak diaphragm system. The pressure in the main chamber was UHV level ( $\approx 10^{-7}$  mbar). Calibration of the mass spectrometer signal was performed based on mixtures of known composition. For all experiments, gas-phase

composition was calculated from the mass spectrometer signal at *m/e* ratios of 44, 60, 58, 28, 16, 26, 27, 41, 2 for  $\text{CO}_2$ ,  $\text{CH}_3\text{COOH}$ ,  $(\text{CH}_3)_2\text{CO}$ ,  $\text{CO}$ ,  $\text{CH}_4$ ,  $\text{C}_2\text{H}_4$ ,  $\text{C}_2\text{H}_6$ ,  $\text{C}_3\text{H}_6$  and  $\text{H}_2$ , respectively. Fragmentation of the different species was calibrated and contributions from other than the indicated ones were subtracted, as well as the background level.

#### 2.2.2. Steady-state and kinetic experiments

Steady-state experiments were carried out using an apparatus which consists of a flow system, the reactor unit and the analysis system. The flow system consists of four mass flow controllers (MKS Instruments) for the regulation of gas flow and an HPLC pump (Marathon, Scientific Systems) for the liquid flow. The reactants are fed to a micro-reactor which is placed into an electric furnace. The analysis system comprises of two gas chromatographs (GC 14A and GC-8B, Shimadzu) and a mass spectrometer (OmniStar GSD 300, Balzers) connected in parallel through a common set of switch valves. The specific apparatus, the experimental procedure and the analytical procedure have been described in detail in a previous communication [22].

### 2.3. Experimental procedures

#### 2.3.1. Adsorption of HAc and temperature-programmed desorption (TPD)

Prior to any experiment the catalyst samples were reduced *in situ* under  $\text{H}_2$  flow ( $40 \text{ cm}^3/\text{min}$ ) at  $750^\circ\text{C}$  for approximately 2 h. After purging with He for 15 min, the sample was cooled under He flow to room temperature. At this point ca.  $30 \text{ cm}^3/\text{min}$  of a mixture consisting of 0.5% HAc/He was directed into the reactor chamber. Adsorption took place for 20 min at atmospheric pressure at room temperature. After purging for 15 min with He, a linear temperature ramp ( $15^\circ\text{C}/\text{min}$ ) was initiated. The temperature ramp was terminated at  $750^\circ\text{C}$  and this temperature was maintained for an additional 15 min.

#### 2.3.2. Temperature-programmed reaction (TPR)

After *in situ* reduction of the catalyst under  $\text{H}_2$  flow ( $40 \text{ cm}^3/\text{min}$ ) at  $750^\circ\text{C}$  for 1 h and purging with He for 15 min, the sample was cooled under He flow to room temperature. At this point ca.  $30 \text{ cm}^3/\text{min}$  of a mixture consisting of 0.5% HAc/1.5%  $\text{H}_2\text{O}/\text{He}$  was directed into the reactor chamber. These conditions were achieved by controlling the flow of three independent He lines, two of which passed through saturators with acetic acid and water. The catalyst was kept at room temperature for the first 5 min. After this period, the reactor temperature was increased rapidly (at about 1 min) to  $140^\circ\text{C}$  and continued increasing with a linear rate of  $\beta = 15^\circ\text{C}/\text{min}$ , up to  $750^\circ\text{C}$ .

#### 2.3.3. Titration of deposited carbon (TPO)

The amount of carbon deposited was estimated by temperature-programmed oxidation (TPO) experiments. TPOs followed steady-state reactions for 2 h under various experimental conditions. During reaction, the catalyst was exposed to a mixture (0.5% HAc and 1.5%  $\text{H}_2\text{O}$  in He) of total flow of

30 cm<sup>3</sup>/min, at temperatures of 500 and 700 °C. After purging with He for 15 min and cooling to room temperature, TPO with 1% O<sub>2</sub>/He was initiated with a heating rate of 15 °C/min, during which the response of O<sub>2</sub>, CO and CO<sub>2</sub> were monitored.

#### 2.3.4. Temperature-programmed reduction with CO (TPR CO)

After *in situ* reduction of the catalyst under H<sub>2</sub> flow (40 cm<sup>3</sup>/min) at 300 °C for 1 h and purging with He for 15 min, the sample was cooled under He flow to room temperature. At this point, 40 cm<sup>3</sup>/min of a mixture consisting of 0.25% CO/He was directed into the reactor. The catalyst was kept at room temperature for 10 min, followed by a temperature ramp to 750 °C with a linear rate of 30 °C/min. Evolution of CO and CO<sub>2</sub> in the gas phase was followed by mass spectrometer.

#### 2.3.5. Ammonia adsorption and temperature-programmed desorption

The acidity of the two carriers on which the Ru catalysts are supported (MgAl and Al<sub>2</sub>O<sub>3</sub>) was investigated in the present study by NH<sub>3</sub> adsorption at room temperature. Prior to any experiment, the samples were treated at 600 °C for 1 h under He flow and then oxidized with 20% O<sub>2</sub>/He flow at 400 °C for 30 min. After purging with He for 10 min, the sample was cooled under He flow to room temperature. At this point ca. 40 cm<sup>3</sup>/min of a mixture consisting of 0.52% NH<sub>3</sub>/He was directed into the reactor chamber. Adsorption took place for 30 min at atmospheric pressure at room temperature. After purging for 10 min with He, a linear temperature ramp (30 °C/min) was initiated. The temperature ramp was terminated at 750 °C and this temperature was maintained for an additional 10 min.

### 3. Results and discussion

#### 3.1. Characterization of catalysts and supports

BET surface areas of fresh carriers and catalysts are reported in Table 1. As expected, the surface area of Al<sub>2</sub>O<sub>3</sub> is reduced upon addition of MgO and Ru. Two Al<sub>2</sub>O<sub>3</sub> carriers with different surface areas were used for the preparation of the Ru catalysts, resulting in the attainment of similar surface areas between these two catalysts (79.0 and 81.3 m<sup>2</sup>/g, Table 1). Metal dispersion of the two Ru catalysts, as measured by hydrogen chemisorption, is also reported in Table 1. Metal dispersion of the Ru/MgO/Al<sub>2</sub>O<sub>3</sub> catalyst is somewhat higher compared to the Ru/Al<sub>2</sub>O<sub>3</sub> catalyst. The average size of the Ru

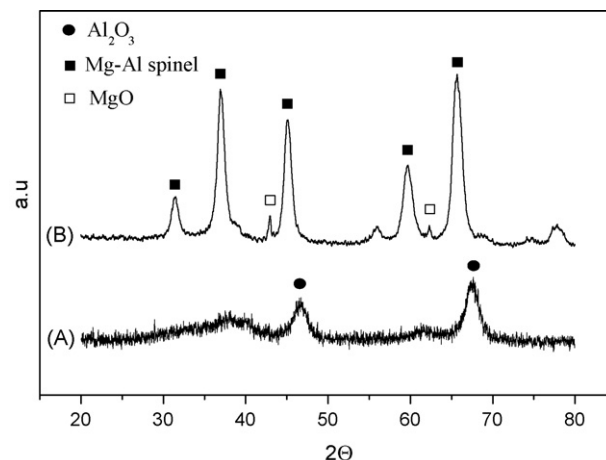


Fig. 1. XRD pattern of Al<sub>2</sub>O<sub>3</sub> carrier (A) and of MgO/Al<sub>2</sub>O<sub>3</sub> carrier (B).

crystallites, also reported in Table 1, is rather similar, in the neighbourhood of 8–10 nm.

The two carriers were also investigated by X-ray diffraction. The X-ray diffractograms of the magnesia/alumina support as well as that of the initial alumina carrier are presented in Fig. 1. XRD lines of the MgO/Al<sub>2</sub>O<sub>3</sub> carrier are very close to the Mg<sub>0.388</sub>Al<sub>2.408</sub>O<sub>4</sub> spinel (ICDD file no. 76-0306), as also Aupretre et al. [24] have observed. Other investigators have noticed that upon addition of amounts of MgO to Al<sub>2</sub>O<sub>3</sub> similar to those used in the present study, an outer layer of MgAl<sub>2</sub>O<sub>4</sub> spinel was formed and phases of both γ-Al<sub>2</sub>O<sub>3</sub> and MgAl<sub>2</sub>O<sub>4</sub> were detected by XRD [25]. However, it is obvious from Fig. 1 that no traces of γ-Al<sub>2</sub>O<sub>3</sub> are detected in the present study. In contrast, minute amounts of MgO are detected in the support, as the appearance of two peaks at 42.9° and 62.3° (ICDD file nos. 04-0829 and 45-0946) imply. This fact can lead to the conclusion that the solid-state reaction of alumina with magnesium oxide is complete, and the support is in the form of Mg<sub>0.388</sub>Al<sub>2.408</sub>O<sub>4</sub> spinel, in which the entire amount of Al is present, while the excess magnesium is present as MgO. This support was also characterized by EDS analysis, the results of which are listed in Table 2. From the listed values, taking into account the previous hypothesis, it can be calculated that the support is comprised of ~94 wt.% magnesium aluminate spinel and ~6% of magnesium oxide. Results of the EDS analysis for the Ru catalysts are also presented in Table 2.

The average spinel crystal size derived from the Debye–Scherrer equation, based on the most intense peaks ({3 1 1} at 37.0° and {4 0 0} at 45.1°), is 8.8 nm, consistent with the results of Aupretre et al. [24].

Table 1

BET surface areas of carriers and catalysts, Ru dispersion of fresh catalysts and Ru crystallite size

Materials	BET surface area (m <sup>2</sup> /g)	Metal dispersion (%)	Crystallite size (nm)
Al <sub>2</sub> O <sub>3</sub>	148.2	–	–
MgO/Al <sub>2</sub> O <sub>3</sub>	85.7	–	–
5% Ru/Al <sub>2</sub> O <sub>3</sub>	79.0	8.8	10.8
5% Ru/MgO/Al <sub>2</sub> O <sub>3</sub>	81.3	12.0	8.0

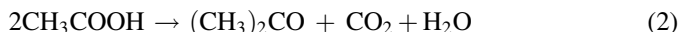
Table 2

EDS analysis of carriers and catalysts

Materials	Elementary analysis (wt.%)			
	Al	Mg	O	Ru
MgO/Al <sub>2</sub> O <sub>3</sub>	44.04	9.91	46.55	–
Ru/Al <sub>2</sub> O <sub>3</sub>	49.12	–	45.28	5.46
Ru/MgO/Al <sub>2</sub> O <sub>3</sub>	41.45	9.32	44.2	5.03

### 3.2. Temperature-programmed desorption (TPD) of adsorbed acetic acid

The interaction of HAc with the surfaces of  $\text{Al}_2\text{O}_3$  and  $\text{MgO}/\text{Al}_2\text{O}_3$  (hitherto referred to as MgAl, for shortness), and the corresponding Ru catalysts was investigated by adsorption of HAc on these materials, followed by temperature-programmed desorption. The TPD spectrum observed over the  $\text{Al}_2\text{O}_3$  carrier is shown in Fig. 2A. A large HAc desorption peak dominates the spectrum at low temperatures (about 150 °C). This is due to the large adsorption capacity of  $\text{Al}_2\text{O}_3$ . The molecularly desorbing HAc is followed by  $\text{CO}_2$  evolution, although in small amounts.  $\text{CO}_2$  may be originating from the ketonization reaction:



while the acetone produced is retained adsorbed on the surface of the carrier. The ketonization reaction is taking place with much higher rates within the temperature range of 350–450 °C, producing carbon dioxide and acetone. Within this temperature range acetone is further decomposed, mainly to  $\text{C}_3\text{H}_6$ , while

trace amounts of  $\text{CH}_4$ ,  $\text{H}_2$  and  $\text{CO}$  are formed at higher temperatures (above 600 °C).

The TPD spectrum observed over the MgAl carrier is shown in Fig. 2B. Again, a large amount of adsorbed HAc is desorbed molecularly at low temperatures. The total amount of HAc adsorbed seems to be smaller than that adsorbed on  $\text{Al}_2\text{O}_3$  (Fig. 2A). However, the amount adsorbed per unit surface area is similar in both cases ( $1.09 \mu\text{mol HAc}/\text{m}^2$  for  $\text{Al}_2\text{O}_3$  and  $1.18 \mu\text{mol HAc}/\text{m}^2$  for MgAl).

Two HAc desorption peaks exist in the spectrum: one at approximately 100 °C and a second one at 200 °C. The second peak is also followed by a shoulder. It is apparent that, on this carrier, there are multiple HAc adsorption sites of variable adsorption strength. This fact can be attributed to the magnesium aluminate spinel as well as to the presence of MgO on the carrier. It has been found that HAc adsorption on MgO is promoted by the strong basicity (ionicity) of magnesium oxide, despite its high lattice energy [26]. Mekheimer et al. [27] observed that HAc adsorbed on MgO is desorbed at about 225 °C, which is in agreement with the second peak of Fig. 2B. Thus, the low temperature ( $\sim 100$  °C) desorption peak is attributed to HAc desorbing from spinel sites

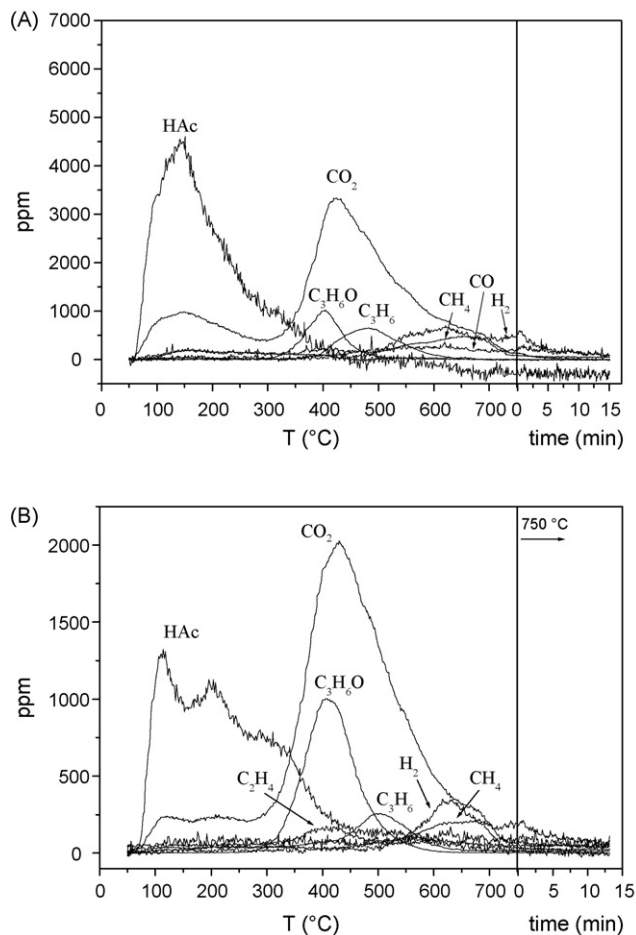


Fig. 2. TPD spectra obtained following adsorption of acetic acid at room temperature from 0.5% HAc in He mixture on  $\text{Al}_2\text{O}_3$  (A) and  $\text{MgO}/\text{Al}_2\text{O}_3$  (B) carriers. Experimental conditions—mass of catalyst: 100 mg; particle size: 0.18–0.25 mm; flow rate:  $\sim 30 \text{ cm}^3/\text{min}$ ;  $\beta = 15 \text{ }^\circ\text{C}/\text{min}$ ;  $P = 1 \text{ atm}$ .

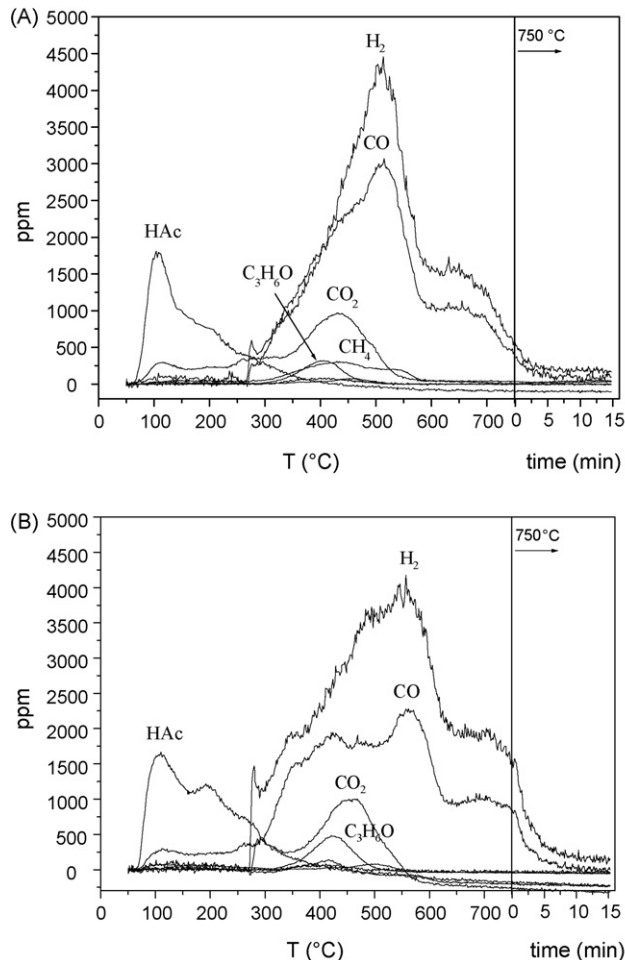


Fig. 3. TPD spectra obtained following adsorption of acetic acid at room temperature from 0.5% HAc in He mixture on  $\text{Ru}/\text{Al}_2\text{O}_3$  (A) and  $\text{Ru}/\text{MgO}/\text{Al}_2\text{O}_3$  (B) catalysts. Experimental conditions: same as Fig. 2.

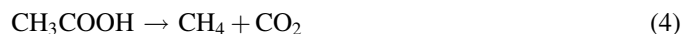
and the high temperature ( $\sim 200^\circ\text{C}$ ) peak is attributed to HAc desorbing from MgO sites. However, as indicated earlier, MgO is only 6% of the carrier, while the desorption peak of HAc is rather large. This means that either the capacity of MgO for HAc adsorption is very high, or that other HAc adsorption sites, formed by the addition of MgO to  $\text{Al}_2\text{O}_3$ , contribute to this peak. Such sites could be at the interface between MgO and spinel particles.

As in the alumina case, the ketonization reaction is initiated at low temperature with very low rates and it is accelerated at approximately  $320^\circ\text{C}$ , producing acetone and carbon dioxide according to Eq. (2). These two products present maxima at  $420^\circ\text{C}$ , in agreement with the literature [28]. However, the concentration of acetone is about half of that of  $\text{CO}_2$ , implying that acetone is maintained on the carrier surface and it is decomposed at higher temperatures, as is indicated by the presence of  $\text{C}_3\text{H}_6$ ,  $\text{CH}_4$  and  $\text{H}_2$ . Of course, acetone may be undergoing further oligomerization reactions via intermediates, such as mesityl oxide, ketene, etc. [18,29]. Small amounts of  $\text{CH}_4$  and  $\text{H}_2$  are present at higher temperatures (above  $550^\circ\text{C}$ ), probably due to acetone decomposition, as mentioned above, or due to cracking reactions of  $\text{C}_3\text{H}_6$ .

Identical TPD experiments conducted over Ru catalysts produced very different spectra, as can be seen in Fig. 3A and B. In the  $\text{Ru}/\text{Al}_2\text{O}_3$  case (Fig. 3A), a large HAc desorption peak, having the same characteristics as that of Fig. 2A, dominates the spectrum at low temperatures. Thus, ruthenium is not active in this temperature range. However, at temperatures above  $260^\circ\text{C}$ , hydrogen and carbon monoxide are produced at high rates, most probably due to the decomposition reaction:



$\text{CO}$  and  $\text{H}_2$  show exactly the same trend, quantitatively according to Eq. (3), up to approximately  $420^\circ\text{C}$ . At higher temperatures, the concentration of  $\text{CO}$  is less than that of  $\text{H}_2$ , which may be attributed to reforming and/or decomposition reactions of adsorbed species which lead to evolution of  $\text{H}_2$  and carbon deposits or  $\text{CO}_2$ . At temperatures above  $300^\circ\text{C}$ , other reactions also take place as witnessed by the presence of  $\text{CO}_2$ ,  $\text{C}_3\text{H}_6\text{O}$  and  $\text{CH}_4$ . Acetone and carbon dioxide are formed via the ketonization reaction (Eq. (2)), while  $\text{CH}_4$  is produced, most probably, via the following reactions:



The production of  $\text{H}_2\text{O}$  via reaction (2) results in further hydrogen production, via reforming reactions of HAc,  $\text{CH}_4$  or other adsorbed species or via the WGS reaction:



which also contributes to the higher  $\text{H}_2$  concentration, as compared to that of  $\text{CO}$ .

The TPD spectrum obtained over the  $\text{Ru}/\text{MgAl}$  catalyst is presented in Fig. 3B. The large HAc desorption peak at low temperatures is also present in this case. As in the  $\text{MgAl}$  case (Fig. 2B), two peaks of desorbing HAc exist in the TPD

spectrum of the Ru catalyst. Again, reaction (3) dominates the spectrum, producing  $\text{CO}$  and  $\text{H}_2$  at approximately equal amounts up to  $400^\circ\text{C}$ . Above this temperature, the concentration of  $\text{CO}$  is less than that of  $\text{H}_2$ , for the reasons discussed above. However, the difference between the quantities of  $\text{H}_2$  and  $\text{CO}$  produced is larger in this case, as compared to that of Fig. 3A. This may be due to the production of higher amounts of  $\text{H}_2\text{O}$  via the ketonization reaction (Eq. (2)) and the imminent formation of hydrogen via steam-reforming reactions. Also, the larger  $\text{H}_2$  concentration may be related to the enhanced mobility of  $\text{OH}^-$  anions which is observed over this catalyst, as compared to the  $\text{Ru}/\text{Al}_2\text{O}_3$  one. This results in further hydrogen production via reactions of hydroxyl groups with HAc and/or other adsorbed species (reforming reactions). The spillover phenomenon of O and/or  $\text{OH}^-$  ions is discussed in a latter section. The ketonization reaction takes place over the temperature range of  $350\text{--}500^\circ\text{C}$ , at a somewhat larger extent as compared to Fig. 3A. The reason for this is the presence of MgO on the carrier which is a basic oxide. Basic oxides are generally thought to be more active in the ketonization reaction than acidic ones [28–30]. A difference between the TPD spectra

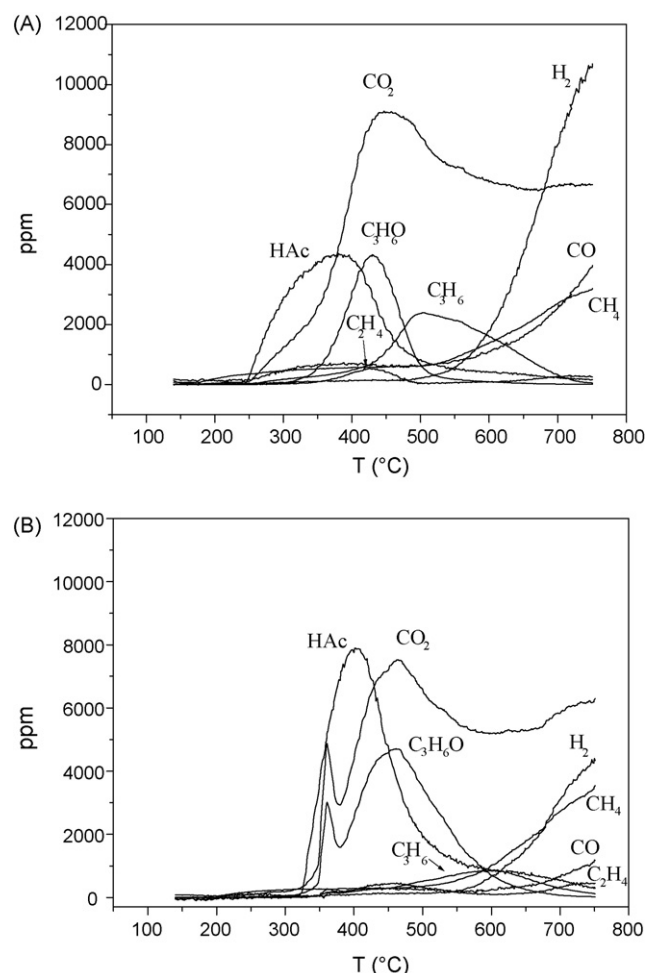


Fig. 4. Spectra of temperature-programmed reaction obtained under steam-reforming conditions over  $\text{Al}_2\text{O}_3$  (A) and  $\text{MgO}/\text{Al}_2\text{O}_3$  (B) carriers. Experimental conditions—mass of carrier: 100 mg (5-mm bed); particle size: 0.18–0.25 mm;  $\text{H}_2\text{O}/\text{HAc}$  molar ratio: 3; flow rate:  $\sim 30\text{ cm}^3/\text{min}$ ; feed: 0.5% HAc, 1.5%  $\text{H}_2\text{O}$  in He,  $\beta = 15^\circ\text{C}/\text{min}$ ;  $P = 1\text{ atm}$ .

of the two Ru catalysts is that over the Ru/MgAl catalyst no methane is detected, implying that either reactions (4) and (5) are not promoted in this case, or that  $\text{CH}_4$  is rapidly reacting with the spillover hydroxyl or oxygen anion species mentioned above.

### 3.3. Reaction scheme under steam-reforming conditions in transient mode

The reaction scheme of steam reforming of HAc was investigated by conducting a series of transient experiments in which the reactor was fed with a gaseous mixture consisting of 0.5% HAc, 1.5%  $\text{H}_2\text{O}$ , balance He, while temperature was ramped up to  $750^\circ\text{C}$  at a linear rate of  $15^\circ\text{C}/\text{min}$ . This feed composition gives a steam-to-acetic acid molar ratio of 3:1, which is 50% higher than the stoichiometric ratio for complete steam reforming of HAc (reaction (1)).

The TPR spectrum obtained over the  $\text{Al}_2\text{O}_3$  carrier is shown in Fig. 4A. HAc is totally adsorbed on the alumina surface at low temperatures, and is desorbed at temperatures higher than  $250^\circ\text{C}$ . Activity is initiated at  $250\text{--}300^\circ\text{C}$ , with the ketonization reaction (Eq. (2)) taking place, producing  $\text{CO}_2$  and  $\text{C}_3\text{H}_6\text{O}$ . However, the  $\text{CO}_2$  concentration is significantly larger than that of acetone. This is due to the fact that acetone remains adsorbed on the catalyst surface and it desorbs or reacts further at higher temperatures, as discussed earlier.  $\text{CO}_2$  is also produced by various reformation and oxidation reactions, especially at higher temperatures. Hydrogen production is initiated at approximately  $550^\circ\text{C}$  and its rate increases rapidly with temperature. Hydrogen originates not only from cracking of  $\text{C}_2\text{H}_4$  and  $\text{C}_3\text{H}_6$  but also from reforming of HAc and hydrogen-containing fragments which may be deposited on the  $\text{Al}_2\text{O}_3$  surface. The formation of CO at higher temperatures is due to the reverse WGS reaction (Eq. (6)) or due to reaction (3). Methane is also present at high temperatures, implying that reactions (4) and (5) also take place within this temperature range.

The TPR spectrum obtained over the MgAl carrier is shown in Fig. 4B. HAc is adsorbed on the carrier surface at low temperatures, until the surface is saturated, and is desorbed at higher temperatures (above  $300^\circ\text{C}$ ). For this reason the gas-phase concentration of HAc exceeds the feed concentration (5000 ppm) within a narrow temperature range. HAc is desorbed at about  $50^\circ\text{C}$  higher than in the case of  $\text{Al}_2\text{O}_3$  and with sharper peak, indicating that the HAc adsorption is stronger over the MgAl carrier. No activity is taking place up to  $300^\circ\text{C}$ . The ketonization reaction takes over at the temperature of  $350^\circ\text{C}$  producing acetone and carbon dioxide according to Eq. (2). Concentration of  $\text{CO}_2$  is larger compared to that of acetone, implying that acetone is further reacted, as described earlier (Section 3.2). Hydrogen production is initiated at about  $550^\circ\text{C}$  and its production rate is increased rapidly with temperature. The steam-reforming reaction of HAc (Eq. (1)), as well as reforming of other hydrogen-containing adsorbed fragments is taking place at elevated temperatures. Part of hydrogen is due to cracking reactions of  $\text{C}_3\text{H}_6$  and HAc, via reaction (3) for example, as witnessed by the presence of

amounts of CO. However, the amounts of CO and  $\text{H}_2$  produced are smaller than those over the  $\text{Al}_2\text{O}_3$  case. This may be due to the promotion of reaction (3) in the case of the  $\text{Al}_2\text{O}_3$  carrier, as well as due to the production of smaller amounts of  $\text{C}_3\text{H}_6$  in the present case, and thus the imminent smaller production of  $\text{H}_2$  due to cracking reactions of propylene. At the same temperature range ( $T > 550^\circ\text{C}$ ),  $\text{CH}_4$  is also produced, implying that reactions (4) and/or (5) are also taking place.

Comparison of the TPR spectra of the two carriers can lead to the conclusion that similar reactions take place over these materials and product distribution is more or less the same over the entire temperature range. Carbon dioxide, acetone and propylene are the main products at medium temperatures ( $350\text{--}550^\circ\text{C}$ ), while hydrogen, methane and carbon oxides are produced at higher temperatures.

Comparing the TPD and TPR spectra (Figs. 2 and 4) obtained over the two carriers it seems that the reaction pathway at low and medium temperatures is more or less the same. This implies that within this temperature range, even under HAc steam-reforming conditions, the ketonization reaction along with decomposition reactions of HAc take place and the presence of  $\text{H}_2\text{O}$  has no significant effects on the reaction scheme. However, at higher temperatures the situation

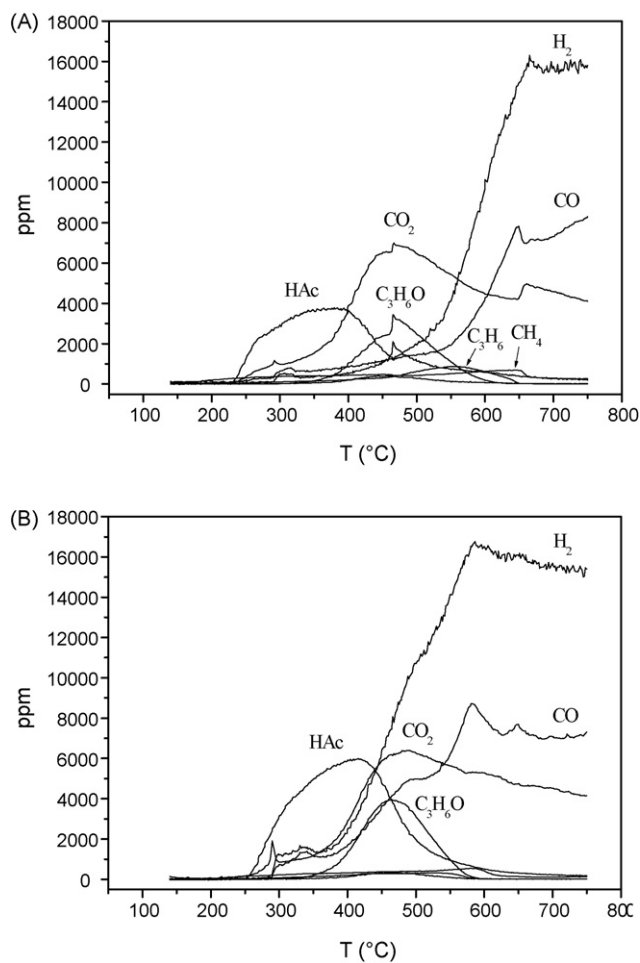


Fig. 5. Spectra of temperature-programmed reaction obtained under steam-reforming conditions over Ru/ $\text{Al}_2\text{O}_3$  (A) and Ru/MgO/ $\text{Al}_2\text{O}_3$  (B) catalysts. Experimental conditions: same as Fig. 4.

seems to be altered and steam-reforming reactions dominate, under conditions of steam reforming of HAc.

Identical experiments were conducted over the two Ru catalysts and the results are presented in Fig. 5A and B. As was already mentioned in Section 3.2, ruthenium is not active at low temperatures. This is also clear in Fig. 5A in which no activity is observed up to 300 °C. HAc is adsorbed at low temperatures and starts to desorb at about 240 °C. The ketonization reaction is initiated at about 350 °C and, from this temperature on, gas-phase concentration of HAc is reduced and disappears at temperatures above 500 °C. CO<sub>2</sub> and C<sub>3</sub>H<sub>6</sub>O exhibits maxima at about 460 °C. Acetone is further decomposed to C<sub>3</sub>H<sub>6</sub> or CH<sub>4</sub>, which are present in small amounts in the temperature range of 500–650 °C, and/or undergoing oligomerization reactions [18,29], resulting in lower concentration, compared to that of CO<sub>2</sub>. Hydrogen production is initiated at about 400 °C and, as expected, its production rate is increased rapidly with temperature. CO is also produced within the same temperature range. At temperatures higher than 550 °C the steam-reforming reaction of HAc (Eq. (1)) along with the reverse WGS reaction (Eq. (6)) dominate the spectrum. As a result, concentration of hydrogen is rapidly increasing, while CO<sub>2</sub> concentration decreases and that of CO increases. At elevated temperature, CH<sub>4</sub>, which is present in small concentrations, is reformed either by steam or by carbon dioxide.

The TPR spectrum obtained over the Ru/MgAl catalyst is shown in Fig. 5B. At low temperatures (up to 300 °C) Fig. 5A and B are nearly identical. A main difference between the two spectra of Fig. 5 is the production of CO and H<sub>2</sub> at high rates at the temperature of 300 °C over the Ru/MgAl catalyst, probably via reaction (3), at approximately 100 °C lower than in the case of Ru/Al<sub>2</sub>O<sub>3</sub> catalyst. However, concentration of H<sub>2</sub> is higher than that of CO (not equal as defined by stoichiometry of Eq. (3)), implying that the WGS reaction (Eq. (6)) and/or HAc steam-reforming reaction (Eq. (1)) are taking place within this temperature range (350–500 °C), resulting in further production of H<sub>2</sub> and CO<sub>2</sub>. This is confirmed also by the enhanced CO<sub>2</sub> concentration, as compared to that of acetone. No or very small amounts of C<sub>3</sub>H<sub>6</sub> or CH<sub>4</sub> are observed over this catalyst, implying that either no decomposition reactions of acetone take place, or that these molecules react rapidly. This explains the relatively small difference between the concentrations of acetone and carbon dioxide produced. As mentioned already, the most important difference between the two spectra of Fig. 5 pertains to hydrogen production. Over the Ru/MgAl catalyst, hydrogen production is initiated at about 100 °C lower than in the case of Ru/Al<sub>2</sub>O<sub>3</sub> catalyst. Also, hydrogen concentration reaches its maximum at the temperature of 590 °C, which is 60–70 °C lower than in the case of Ru/Al<sub>2</sub>O<sub>3</sub>. At this temperature, concentrations of H<sub>2</sub> and CO exhibit peaks which may be due to reaction of excess steam with carbonaceous species deposited on the catalyst surface. At temperatures above 600 °C, CO, CO<sub>2</sub> and H<sub>2</sub> are the only products which are observed, implying that steam reforming of HAc, along with the WGS reaction takes place at this temperature range.

The main difference between the performances of the two ruthenium catalysts pertains to hydrogen production, with Ru/

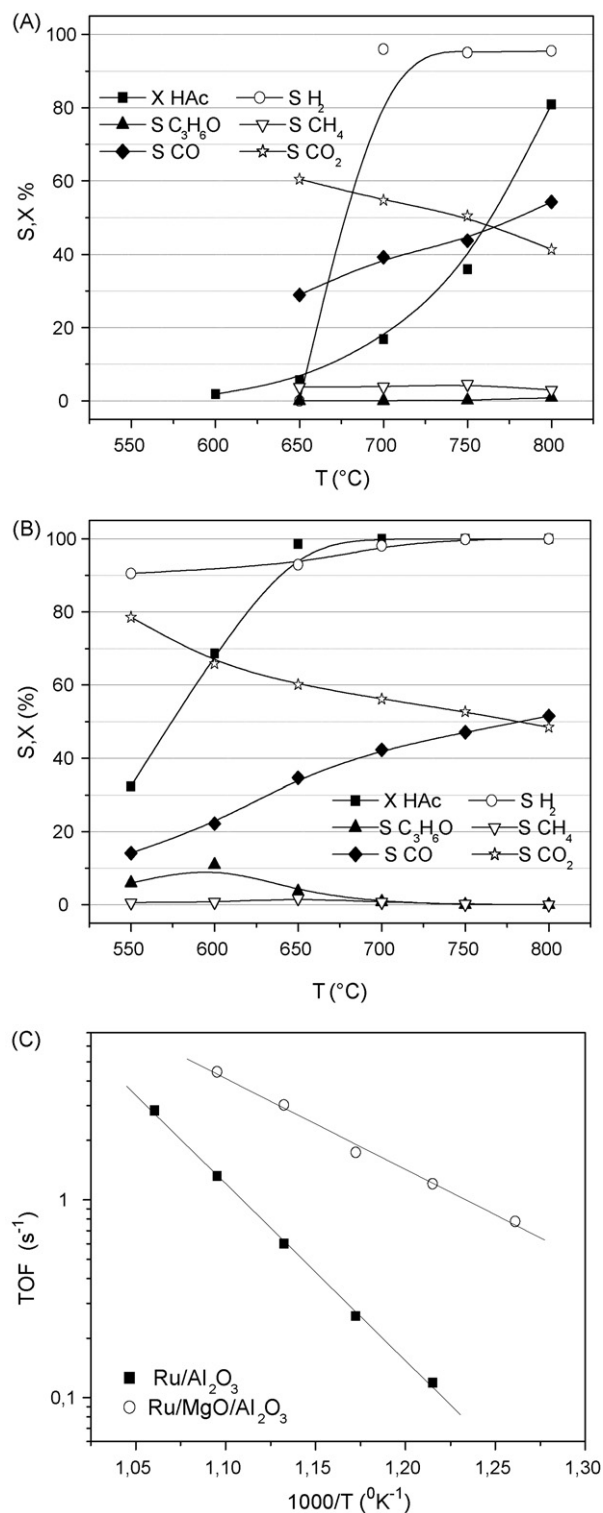


Fig. 6. HAc conversion and product distribution under steady-state conditions over 5% Ru/Al<sub>2</sub>O<sub>3</sub> (A) and 5% Ru/MgO/Al<sub>2</sub>O<sub>3</sub> (B) catalysts, and Arrhenius plot of turnover frequencies of HAc conversion over these catalysts (C). Experimental conditions—mass of catalyst: 100 mg; particle size: 0.18–0.25 mm; H<sub>2</sub>O/HAc molar ratio: 3; flow rate = 290 cm<sup>3</sup>/min; feed: 7.5% HAc, 22.7% H<sub>2</sub>O in He; *P* = 1 atm.

MgAl being more active, as compared to Ru/Al<sub>2</sub>O<sub>3</sub>. Enhanced formation of hydrogen over Ru/MgAl was also observed in the TPD experiments. However, a similar phenomenon was not observed with carriers only (with no ruthenium). Thus, it is reasonable to assume that the enhanced activity of Ru/MgAl catalyst is due to an interaction between the metal particles and the carrier. This issue is discussed in detail in Section 3.5.

### 3.4. Catalytic performance of the Ru catalysts under steady-state conditions

The performance of the Ru/Al<sub>2</sub>O<sub>3</sub> and Ru/MgAl catalysts with respect to reaction temperature was also investigated under steady-state conditions. Results of HAc conversion and product distribution as a function of reaction temperature are presented in Fig. 6A and B for the 5% Ru/Al<sub>2</sub>O<sub>3</sub> and 5% Ru/MgAl catalysts, respectively.

In the case of Ru/Al<sub>2</sub>O<sub>3</sub> catalyst (Fig. 6A), under the present experimental conditions, HAc is not fully reacted even at temperatures as high as 800 °C. The main products which are observed in the gas phase are H<sub>2</sub>, CO and CO<sub>2</sub>, while CH<sub>4</sub> is also present in the entire temperature range but in small amounts. Thus, the main reactions which take place are the HAc reforming (Eq. (1)) along with the WGS reaction (Eq. (6)). Hydrogen selectivity is at high levels (above 90%) at temperatures higher than 700 °C, while H<sub>2</sub> is not detected at lower temperatures. Formation of CO is favoured at higher temperatures, in contrast to CO<sub>2</sub>, according to the WGS limitations. The methanation reactions (Eqs. (4) and (5)) also occur over the entire temperature range, as the presence of CH<sub>4</sub> indicates, but with very low rates.

Catalytic activity is much higher in the case of Ru/MgAl catalyst (Fig. 6B). Complete conversion of HAc and 100% selectivity towards H<sub>2</sub> production is observed at temperatures above 700 °C. Carbon oxides are the only other products at this temperature range. At temperatures below 650 °C acetone is observed, resulting in reduced hydrogen selectivity. This implies that in this temperature range, the ketonization reaction (Eq. (2)) occurs simultaneously with the steam-reforming (Eq. (1)) and WGS reactions (Eq. (6)). Finally, CH<sub>4</sub> is observed only in trace amounts over this temperature range.

Comparison between Fig. 6A and B leads to the conclusion that the 5% Ru/MgAl catalyst exhibits significantly higher activity as compared to the 5% Ru/Al<sub>2</sub>O<sub>3</sub> catalyst. The same conclusion was reached under conditions of steam reforming of the water-soluble fraction of real bio-oil [20] indicating that the use of a model compound, such as acetic acid, may be a good approximation of catalytic performance under more realistic conditions.

A better means of comparing catalytic activity of different catalysts is turnover frequency, which is activity expressed per exposed metal atom. Turnover frequencies of HAc conversion were determined from experiments in which HAc conversion was maintained below 10% (initial rates), taking into account the dispersion of the catalysts, as estimated by selective chemisorption of H<sub>2</sub> (Table 1). Results are presented in the Arrhenius-type diagram of Fig. 6C, where the TOFs of each

catalyst are plotted as functions of the inverse reaction temperature. It is clear from this diagram as well, that the 5% Ru/MgAl catalyst presents much higher intrinsic activity than the 5% Ru/Al<sub>2</sub>O<sub>3</sub> catalyst. It must be noted, however, that the addition of MgO on Ru/Al<sub>2</sub>O<sub>3</sub> catalyst is not associated with major changes in the reaction network or with significant alteration of product distribution, as discussed earlier. Thus, it is reasonable to assume that the observed enhanced activity is due to an interaction between the metal particles and the carrier, most probably at the interface between the two solids.

### 3.5. The role of MgO in the Ru/MgAl catalyst

The enhanced steam-reforming activity of the Ru/MgAl catalyst, as compared to the Ru/Al<sub>2</sub>O<sub>3</sub> catalyst, and the role of MgO in the catalytic process should be assessed with respect to mechanistic aspects of the catalytic system. It has been proposed [13,31] that the reaction mechanism of steam reforming of oxygenates consists of two important reaction pathways: in the first one, the oxygenate is primarily dissociated on the metal, leading to adsorbed hydrocarbon fragments. In the second pathway, steam adsorption and dissociation occurs, mainly on the support surface. The resulting –OH groups migrate onto the metal particles through the metal/support interface. Once on the metal, they react rapidly with hydrocarbon fragments to give CO, CO<sub>2</sub> and H<sub>2</sub>. The ability of the catalyst to keep the metal surface clean through O and/or –OH spillover processes seems to be an important step toward catalytic activity.

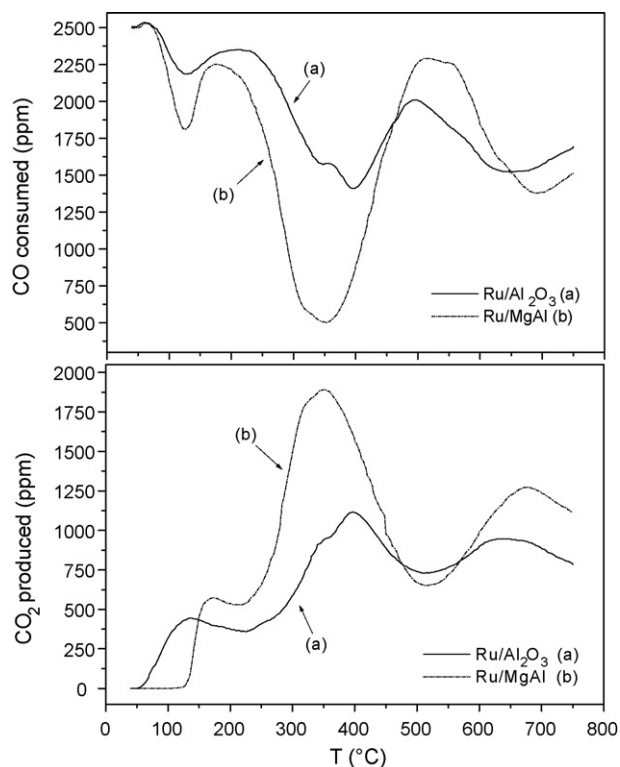


Fig. 7. CO and CO<sub>2</sub> responses of TPR with CO of Ru/Al<sub>2</sub>O<sub>3</sub> and Ru/MgO/Al<sub>2</sub>O<sub>3</sub> catalysts. Experimental conditions—mass of catalyst: 150 mg; total flow: 40 cm<sup>3</sup>/min, feed: 0.25% CO/He,  $\beta$  = 30 °C/min,  $P$  = 1 atm.

To address this issue the spillover process of O and/or –OH groups over the Ru catalysts was investigated in the present study, in an indirect manner, by conducting temperature-programmed reaction experiments, using CO as the reactant (TPR CO). Since CO oxidation takes place on the surface of the metal particles only, the oxidation of CO (in the absence of gas-phase oxygen) can be safely attributed to spillover of O and/or –OH species migrating on the metal surface through the three-phase boundary. TPR experiments were conducted over the Ru/MgAl and the Ru/Al<sub>2</sub>O<sub>3</sub> catalysts, and the oxidation of CO was used to monitor the process of oxygen and/or hydroxyl anion spillover onto the metal particles. The resulting TPR spectra are shown in Fig. 7, where the CO consumed and the CO<sub>2</sub> produced are plotted with respect to temperature, for each catalyst. Since, at the start of the experiment, the metal is in its reduced state and the entire surface of the catalyst is free of any adsorbed oxygen (see Section 2.3.4), the production of CO<sub>2</sub>, which occurs simultaneously with the consumption of CO (Fig. 7), is attributed to the reaction of CO with O and/or –OH anions which spillover from the support onto the metal surface. It must be stated that (a) it was established that the support alone is not capable of oxidizing CO within the temperature range investigated and (b) the Boudouard reaction ( $2\text{CO} \rightarrow \text{CO}_2 + \text{C}$ ) is not taking place at any appreciable extent since no carbon was detected on the metal surface, after completion of the TPR CO experiments.

It is obvious from Fig. 7 that CO<sub>2</sub> evolution follows closely CO consumption, indicating that CO oxidation (via WGS and oxidation reactions) is the only source of CO<sub>2</sub> production. Three peaks of CO consumed are present in the TPR spectrum: one at low temperatures ( $\sim 120^\circ\text{C}$ ), a second at intermediate temperatures ( $\sim 350^\circ\text{C}$ ), and a third one at high temperatures ( $\sim 700^\circ\text{C}$ ). Similar patterns of TPR CO experiments have also been reported by Katsaounis et al., under conditions of CO oxidation over Pt catalysts [32,33]. They attributed the low temperature peak to CO oxidation by gas-phase oxygen, while the other two peaks (at higher temperatures) to the oxidation of CO by lattice oxygen, designated as  $\beta_2$  and  $\beta_3$  states [32,33]. In the present case, the first small peak at  $120^\circ\text{C}$  is attributed to the reduction of a small quantity of metal which is still in the oxidized state, while the other two peaks (at  $350$  and  $700^\circ\text{C}$ ) are attributed to the oxidation of CO on the surface of Ru particles by lattice oxygen of the  $\beta_2$  and  $\beta_3$  states which diffuses onto the metal surface. Although the total surface areas as well as the ruthenium dispersion of the two catalysts are very close (Table 1), the amount of CO<sub>2</sub> produced over the Ru/MgAl catalyst is significantly higher than the corresponding amount produced over the Ru/Al<sub>2</sub>O<sub>3</sub> catalyst. Integration of the curves of Fig. 7 reveals that the amount of CO<sub>2</sub> produced over the Ru/MgAl catalyst is  $3.5 \mu\text{mol CO}_2/\text{m}^2$  and that over the Ru/Al<sub>2</sub>O<sub>3</sub> catalyst  $2.5 \mu\text{mol CO}_2/\text{m}^2$ . The difference between these two values is about 40%, and it can be attributed to enhanced spillover of O and/or –OH anions from the carrier surface onto the surface of the metal particles, caused by the magnesium aluminate spinel carrier.

The acid/base characteristics of the support are also known to affect the activity and selectivity of the catalyst [34,35], as

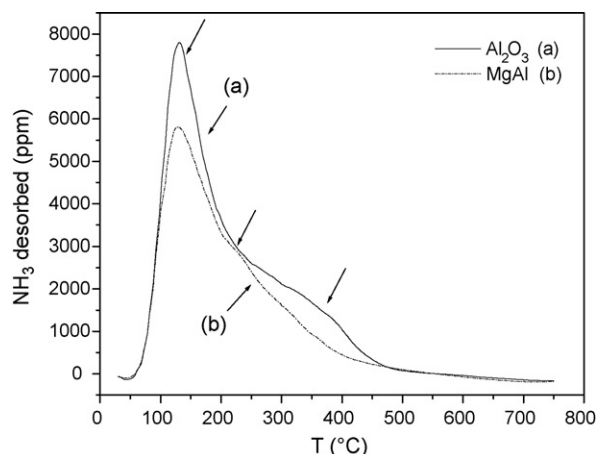


Fig. 8. TPD spectra obtained following adsorption of NH<sub>3</sub> at room temperature from 0.52% NH<sub>3</sub> in He mixture on Al<sub>2</sub>O<sub>3</sub> (A) and MgO/Al<sub>2</sub>O<sub>3</sub> (B) carriers. Experimental conditions—mass of carriers: 200 mg; particle size: 0.18–0.25 mm; flow rate:  $\sim 40 \text{ cm}^3/\text{min}$ ;  $\beta = 30^\circ\text{C}/\text{min}$ ;  $P = 1 \text{ atm}$ .

well as the physicochemical characteristics of the metal supported on the carrier, i.e. metal dispersion [35,36]. The acidity of the two carriers, upon which the Ru crystallites were dispersed (MgAl and Al<sub>2</sub>O<sub>3</sub>), was investigated by conduction of temperature-programmed desorption experiments, following NH<sub>3</sub> adsorption on the carriers at room temperature. Such methods which are based on the interaction of probe molecules, such as NH<sub>3</sub>, with the catalyst surface by temperature-programmed desorption have been extensively used [37–39], due to the intrinsic simplicity of the method.

The resulting TPD spectra are shown in Fig. 8, where NH<sub>3</sub> desorbed is shown as a function of temperature, for each carrier. A major peak at about  $130^\circ\text{C}$  dominates the TPD spectra of both carriers. This peak is followed by a shoulder. In the case of MgAl carrier, the shoulder is probably due to the contribution of a second ammonia desorption peak, with a maximum at about  $230^\circ\text{C}$ , while in the Al<sub>2</sub>O<sub>3</sub> case it seems that the shoulder is due to the contribution of two more peaks, presenting maxima at  $240$  and  $350^\circ\text{C}$ , respectively. These peaks ( $130$ ,  $230$  and  $350^\circ\text{C}$ ), which are pointed with arrows in Fig. 8, are attributed to NH<sub>3</sub> chemisorbed on weak, medium and strong acid sites, respectively [37–40]. In the Al<sub>2</sub>O<sub>3</sub> carrier, while the weak sites correspond to the highest concentration, the population of sites of medium and high strength is also significant. In the MgAl carrier, the population of sites of medium and high strength is very small. The total population of the acidic sites which are present in the carriers is associated with the total amount of ammonia desorbed and can be calculated by integration of the NH<sub>3</sub> desorption curves of Fig. 8. The amount of NH<sub>3</sub> desorbed over the MgAl support is  $3.65 \mu\text{mol NH}_3/\text{m}^2$  and that over the Al<sub>2</sub>O<sub>3</sub> carrier  $4.85 \mu\text{mol NH}_3/\text{m}^2$ .

From the above it can be concluded that addition of MgO to Al<sub>2</sub>O<sub>3</sub> carrier results in reduction of total surface acidity, as well as of acid strength. Reduced acidity is known to lead to reduced carbon deposition rate. This is also confirmed by the results presented in the following section.

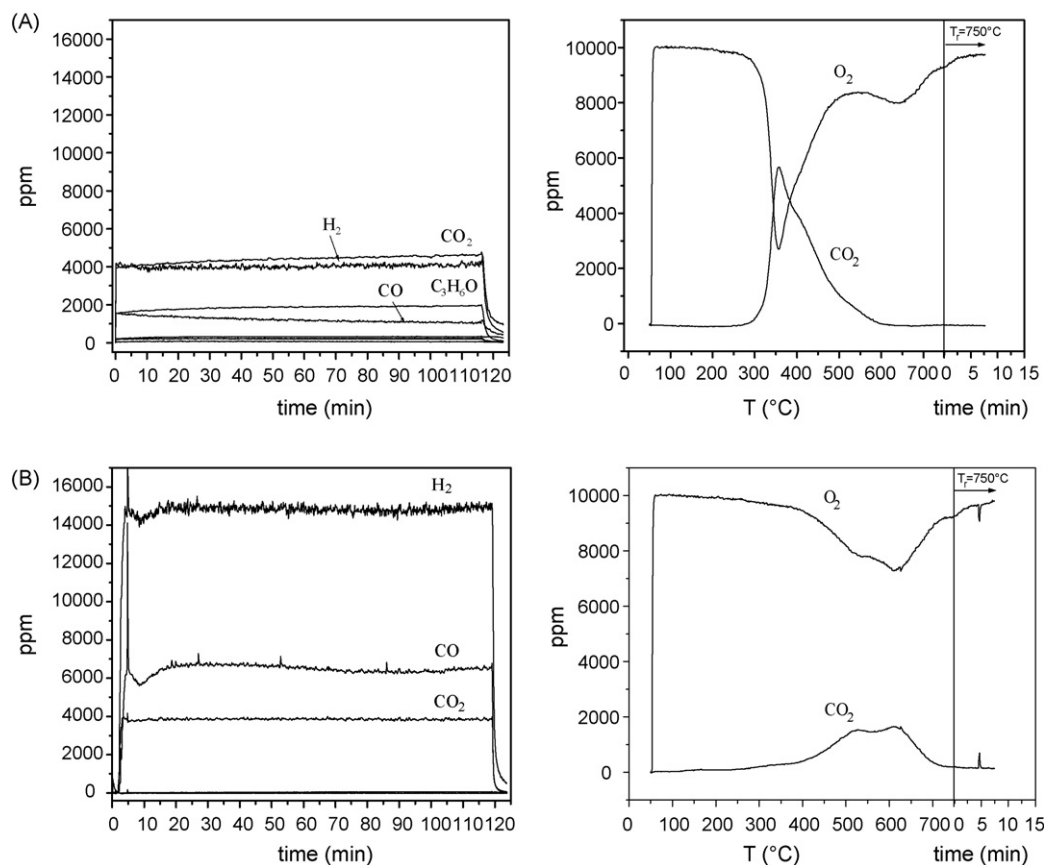


Fig. 9. (Left side): product distribution of steady-state experiment conducted for a period of 2 h (0.5% HAC, 1.5% H<sub>2</sub>O in He,  $F \sim 30 \text{ cm}^3/\text{min}$ ) over the Ru/MgO/Al<sub>2</sub>O<sub>3</sub> catalyst at 500 °C (A) and at 700 °C (B). Experimental conditions—mass of catalyst: 100 mg,  $P = 1 \text{ atm}$ . (Right side): oxygen and CO<sub>2</sub> responses of TPO of carbon deposited on catalyst surface during the corresponding 2 h steady-state experiment. Experimental conditions of TPO: 1% O<sub>2</sub>/He,  $\beta = 15 \text{ }^\circ\text{C}/\text{min}$ .

### 3.6. Estimation of the rate of carbon deposition

Deactivation of supported metal catalysts by carbon and/or coke deposition is a serious problem in steam-reforming processes [41–44]. Carbon deposition was investigated in the present study as a function of reaction temperature and catalyst composition. The amount of carbon deposited on the catalyst surface was estimated by its TPO, following steady-state reaction for 2 h. Product evolution during reaction, as well as carbon oxides evolution and O<sub>2</sub> consumption during the TPO experiment were recorded by mass spectrometer.

Typical reaction and TPO spectra, obtained over the Ru/MgAl catalyst for a feed mixture consisting of 0.5% HAC, 1.5% H<sub>2</sub>O in He, at the temperatures of 500 and 700 °C are shown in Fig. 9A and B, respectively. Although complete conversion of HAC is achieved in both cases, product distribution is different. At the temperature of 500 °C the main products observed are CO, CO<sub>2</sub>, H<sub>2</sub> and C<sub>3</sub>H<sub>6</sub>O. These conditions were chosen in order to produce acetone, since some authors claim that acetone is responsible for the formation of carbonaceous deposits on the catalyst surface via condensation/oligomerization reactions, resulting in deposits [18,44]. On the other hand, at the temperature of 700 °C the only products which were observed are CO, CO<sub>2</sub> and H<sub>2</sub>.

A striking difference between the two TPO spectra (Fig. 9A and B, right side) is the temperature at which CO<sub>2</sub> production is

initiated. In the case of reaction at 500 °C, CO<sub>2</sub> evolves at about 300 °C while its peak is at about 360 °C. In the case of reaction at 700 °C, CO<sub>2</sub> evolution is very low in the temperature range of 300–400 °C, while two peaks are present at about 520 and 620 °C. This implies that different carbon species, probably originating from different sources, are formed. During reaction at 500 °C acetone is produced in sufficient amounts, and thus, the CO<sub>2</sub> peak at 360 °C in the TPO of Fig. 9A, which is absent from the TPO of Fig. 9B, may imply that this carbon originates mainly from acetone. Takanebe et al. [45] claim that acetone is the main source of carbon formation under conditions of HAC steam reforming at 600 °C over Pt/ZrO<sub>2</sub> catalyst. According to these investigators, deposited carbon is in the form of oligomers and it can be removed with oxygen at temperatures below 725 K (452 °C), a fact which is in agreement with the results of the present study.

In the case of reaction at 700 °C two peaks of CO<sub>2</sub> were observed, at 520 and 620 °C. The existence of two peaks of CO<sub>2</sub> production during TPO of coked catalysts has been previously reported [44]. It is generally assumed that the lower temperature peak is due to coke deposited on the metal surface while the higher temperature peak is attributed to coke deposited on the carrier. Moreover, Fatsikostas et al. [3] have observed an identical TPO spectrum over Ni catalyst under conditions of steam reforming of ethanol. They attributed one peak to CH<sub>x</sub> ( $0 < x < 3$ ) species originating from partial or

Table 3

Deviation of oxygen balances of O<sub>2</sub> consumed and CO<sub>2</sub> produced during TPOs for the two Ru catalysts

a/a	Catalysts	Deviations of oxygen balance (%) <sup>a</sup>	
		TPO after reaction at 500 °C	TPO after reaction at 700 °C
1	Ru/Al <sub>2</sub> O <sub>3</sub>	15.5	1.8
2	Ru/MgO/Al <sub>2</sub> O <sub>3</sub>	25.1	3.5

$$^a \text{ Deviation} = \frac{\text{moles O}_{2,\text{consumed}} - \text{moles CO}_{2,\text{formed}}}{\text{moles O}_{2,\text{consumed}}} \times 100.$$

Table 4

Percentages of carbon deposited on catalyst during reaction, based on total carbon fed into the reactor, under steam-reforming conditions at 700 °C and H<sub>2</sub>O/HAc ratio of 3

a/a	Catalysts	% of carbon deposited
1	Al <sub>2</sub> O <sub>3</sub> <sup>a</sup>	47.2 <sup>a</sup>
2	MgO/Al <sub>2</sub> O <sub>3</sub>	22.2
3	Ru/Al <sub>2</sub> O <sub>3</sub>	8.4
4	Ru/MgO/Al <sub>2</sub> O <sub>3</sub>	2.1

<sup>a</sup> Ref. [12].

complete dehydrogenation of C<sub>1</sub> molecules and the other one to polymeric carbon due to ethylene polymerization. However, in the present study ethylene was not detected as reaction product. Furthermore, it was shown in our previous study that carbon deposited on Ni catalyst under conditions of HAc steam reforming is in the graphitic form [12]. Thus, the second peak of CO<sub>2</sub> produced in the TPO spectrum of Fig. 9B is attributed to graphitic carbon, which is deposited on the carrier [12].

To further elucidate the nature of carbon deposits, especially their chemical composition (CH<sub>x</sub>O<sub>y</sub>), material balances of oxygen consumed and CO<sub>2</sub> formed were performed. Of course, part of O<sub>2</sub> is consumed to oxidize the ruthenium catalysts which may be in somewhat reduced state under reaction conditions. However, it is clear from the TPO spectrum of Fig. 9A that ruthenium catalyst is oxidized in the temperature range of 580–750 °C where O<sub>2</sub> is consumed without simultaneous CO<sub>2</sub> production. This amount can be easily estimated and was taken into account in calculations of material balances. This is also true in the Ru/Al<sub>2</sub>O<sub>3</sub> case (not shown). Results of oxygen balances for the two Ru catalysts are summarized in Table 3. A good agreement is observed in the case of TPO following reaction at 700 °C, indicating that only carbon exists on the catalyst surface or that *x* and *y* of the above formulation are essentially 0. In contrast, significant deviation was observed in the case of TPOs after reaction at 500 °C, for both catalysts, since the amount of O<sub>2</sub> which was consumed is higher than that which was evolved as CO<sub>2</sub>. This means that the carbonaceous deposits which are on the catalyst surface are in the CH<sub>x</sub> form, where *x* > 0. This seems to confirm the hypothesis presented in the previous paragraph concerning the nature of carbonaceous deposits on each catalyst.

TPO experiments were conducted for all samples, carriers and catalysts, after reaction for 2 h at 700 °C. The results are summarized in Table 4 in which the percentages (based on total

carbon fed into the reactor) of carbon deposited after 2 h of reaction are shown. It is obvious that catalyst composition plays a major role in coke formation. The alumina carrier strongly favours carbon deposition due to its acidity which favours decomposition and polymerization reactions resulting in the formation of significant amounts of carbonaceous species [40]. Addition of MgO to the Al<sub>2</sub>O<sub>3</sub> carrier results in reduction of the rate of carbon deposition. This may be due to blocking of acid sites (especially strong acid sites) of alumina, as discussed earlier, as well as due to the ability of magnesium to enhance steam adsorption which accelerates carbon gasification. The presence of ruthenium seems to retard the rate of carbon deposition, as compared to the carriers. This is expected due to the fact that ruthenium promotes reforming reactions and inhibits reactions leading to the formation of carbonaceous species, such as decomposition. Comparing the two Ru catalysts, it is clear that less carbon is formed over the Ru/MgAl catalyst.

Finally, the amount of carbon deposited on the Ru catalysts during steady-state experiments (4 h, 750 °C) was also estimated. It was found that, in the case of Ru/Al<sub>2</sub>O<sub>3</sub> catalyst the percentage of carbon deposited (based on total carbon fed into the reactor) was 0.32%, while over the Ru/MgAl catalyst it was 0.11%. These values are in agreement with previous results and confirm the fact that the Ru/MgAl catalyst is more resistant to carbon deposition than the Ru/Al<sub>2</sub>O<sub>3</sub> catalyst.

From the practical point of view, these results indicate that the Ru-based catalysts can be regenerated after prolonged exposure to reforming reaction conditions by burning-off coke. It is known, however, that oxides of ruthenium are rather volatile in presence of excess oxygen. Loss of metal may cause irreversible deactivation of the catalyst. Although we have investigated Ru-based catalysts and their regeneration for many years, we have never observed this phenomenon. A possible explanation is that the small RuO<sub>x</sub> particles which are in close contact with the metal oxide carrier may be less volatile than bulk ruthenium oxides.

#### 4. Summary and conclusions

Ruthenium is one of the most active metals for the steam reforming of HAc. However, the carrier upon which Ru is dispersed plays a major role in defining its catalytic performance. The following conclusions can be deduced from the present study:

- (1) Addition of MgO to Al<sub>2</sub>O<sub>3</sub> results in the formation of a magnesium aluminate spinel of the form Mg<sub>0.388</sub>Al<sub>2.408</sub>O<sub>4</sub>.
- (2) The carriers themselves interact with HAc promoting the ketonization reaction at intermediate temperatures, and reforming and decomposition reactions at higher temperatures.
- (3) The presence of ruthenium on Al<sub>2</sub>O<sub>3</sub> and, especially, on MgAl shifts activity to lower temperatures while hydrogen production occurs at high rates. Ru catalysts promote mainly the ketonization reaction at intermediate tempera-

tures and the steam reforming along with the WGS reactions at elevated temperatures.

- (4) The Ru/MgAl catalyst exhibits higher intrinsic activity as compared to the Ru/Al<sub>2</sub>O<sub>3</sub> catalyst. The enhanced activity seems to be associated with the formation of magnesium aluminate spinel, which offers enhanced O and/or –OH anion spillover from the carrier onto the metal particles and to reduced surface acidity.
- (5) Different carbon species can be formed on the catalytic surface under conditions of steam reforming of HAc, depending on reaction temperature. When reaction is taking place at low temperatures (i.e. 500 °C) CH<sub>x</sub> carbonaceous species are formed originating mainly from acetone, while in the case of 700 °C only carbon exists on the catalytic surface.
- (6) Addition of MgO to Al<sub>2</sub>O<sub>3</sub> carrier has positive effect on carbon deposition. The main reason is the enhanced rate of spillover of O and/or OH<sup>–</sup> radicals, from MgAl carrier onto the Ru particles, and thus enhanced carbon gasification rate.

## Acknowledgment

This work was funded in part by the Commission of the European Community, under contract ENK5-CT-2002-00634.

## References

- [1] M.A. Pena, J.P. Gomez, J.L.G. Fierro, *Appl. Catal. A* 144 (1996) 7.
- [2] A.N. Fatsikostas, D.I. Kondarides, X.E. Verykios, *Chem. Commun.* 9 (2001) 851.
- [3] A.N. Fatsikostas, X.E. Verykios, *J. Catal.* 225 (2004) 439.
- [4] A.N. Fatsikostas, D.I. Kondarides, X.E. Verykios, *Catal. Today* 75 (2002) 145.
- [5] S. Cavallaro, V. Chiodo, A. Vita, S. Freni, *J. Power Sources* 123 (2003) 10.
- [6] G.A. Deluga, J.R. Salge, L.D. Schmidt, X.E. Verykios, *Science* 303 (2004) 993.
- [7] A.V. Bridgwater, *J. Anal. Appl. Pyrol.* 51 (1999) 3.
- [8] A.A. Iordanidis, P.N. Kechagiopoulos, S.S. Voutetakis, A.A. Lemonidou, I.A. Vasalos, *Int. J. Hydrogen Energy* 31 (2006) 1058.
- [9] E.J. Soltes, T.A. Milne, in: A.V. Bridgwater (Ed.), *Fast Pyrolysis of Biomass Handbook*, vol. 2, 1999, p. 243.
- [10] A. Demirbas, *Energy Convers. Manage.* 43 (2002) 1801.
- [11] A. Oasmaa, E. Kuoppala, *Energy Fuels* 17 (2003) 1075.
- [12] A.C. Basagiannis, X.E. Verykios, *Appl. Catal. A* 308 (2006) 182.
- [13] L. Garcia, R. French, S. Czernik, E. Chornet, *Appl. Catal. A* 201 (2000) 225.
- [14] D. Wang, S. Czernik, E. Chornet, *Energy Fuels* 12 (1998) 19.
- [15] D. Wang, D. Montane, E. Chornet, *Appl. Catal. A* 143 (1996) 245.
- [16] S. Czernik, R. French, C. Feik, E. Chornet, *Ind. Eng. Chem. Res.* 41 (2002) 4209.
- [17] C. Rioche, S. Kulkarni, F.C. Meunier, J.P. Breen, R. Burch, *Appl. Catal. B* 61 (2005) 130.
- [18] K. Takanebe, K. Aika, K. Seshan, L. Lefferts, *J. Catal.* 227 (2004) 101.
- [19] P.N. Kechagiopoulos, S.S. Voutetakis, A.A. Lemonidou, I.A. Vasalos, *Energy Fuels* 20 (2006) 2155.
- [20] A.C. Basagiannis, X.E. Verykios, *Catal. Today* 127 (2007) 256.
- [21] C. Branca, P. Giudicianni, C.D. Blasi, *Ind. Eng. Chem. Res.* 42 (2003) 3190.
- [22] A.C. Basagiannis, X.E. Verykios, *Int. J. Hydrogen Energy* 32 (2007) 3343.
- [23] V.A. Tsipourari, A.M. Efstathiou, X.E. Verykios, *J. Catal.* 161 (1996) 31.
- [24] F. Aupretre, C. Descorme, D. Duprez, D. Casanave, D. Uzio, *J. Catal.* 233 (2005) 464.
- [25] J. Guo, H. Lou, H. Zhao, D. Chai, X. Zheng, *Appl. Catal. A* 273 (2004) 75.
- [26] R. Pestman, R.M. Koster, A. van Duijne, J.A.Z. Pieterse, V. Ponc, *J. Catal.* 168 (1997) 265.
- [27] G.A.H. Mekhemer, S.A. Halawy, M.A. Mohamed, M.I. Zaki, *J. Catal.* 230 (2005) 109.
- [28] M. Glinski, J. Kijenski, A. Jakubowski, *Appl. Catal. A* 128 (1995) 209.
- [29] M. Zamora, T. Lopez, R. Gomez, M. Asomoza, R. Melendrez, *Catal. Today* 107/108 (2005) 289.
- [30] M.A. Hasan, M.I. Zaki, L. Pasupulety, *Appl. Catal. A* 243 (2003) 81.
- [31] K. Polychronopoulou, J.L.G. Fierro, A.M. Efstathiou, *J. Catal.* 228 (2004) 417.
- [32] A. Katsaounis, Z. Nikopoulou, X.E. Verykios, C.G. Vayenas, *J. Catal.* 222 (2004) 192.
- [33] A. Katsaounis, Z. Nikopoulou, X.E. Verykios, C.G. Vayenas, *J. Catal.* 226 (2004) 197.
- [34] D.K. Liguras, D.I. Kondarides, X.E. Verykios, *Appl. Catal. B* 43 (2003) 345.
- [35] M.C. Sanchez-Sanchez, R.M. Navarro, J.L.G. Fierro, *Int. J. Hydrogen Energy* 10/11 (2007) 1462.
- [36] J. Vakros, K. Bourikas, C. Kordulis, A. Lycourgiotis, *J. Phys. Chem. B* 107 (2003) 1804.
- [37] F. Arena, R. Dario, A. Parmaliana, *Appl. Catal. A* 170 (1998) 127.
- [38] S.B. Sharma, B.L. Meyers, D.T. Chen, J. Miller, J.A. Dumesic, *Appl. Catal.* 102 (1993) 253.
- [39] H.G. Karge, V. Dondur, J. Weitkamp, *J. Phys. Chem.* 95 (1991) 283.
- [40] W. Xu, S.L. Suib, C. O'Young, *J. Catal.* 144 (1993) 285.
- [41] D.L. Trimm, *Catal. Today* 49 (1999) 3.
- [42] J.R. Rostrup-Nielsen, *Catal. Today* 37 (1997) 225.
- [43] C.H. Bartholomew, *Appl. Catal. A* 212 (2001) 17.
- [44] M. Guisnet, P. Magnoux, *Appl. Catal. A* 212 (2001) 83.
- [45] K. Takanebe, K. Aika, K. Seshan, L. Lefferts, *Chem. Eng. J.* 120 (2006) 133.